J Mater Sci (2010) 45:5502–5511
DOI 10.1007/s10853-010-4608-z

Degradation of 5 mol% yttria–zirconia by intergranular cracking in water at 300 °C

W. Vandermeulen · R.-W. Bosch · A. Leenaers · W. Van Renterghem · F. Snijkers

Received: 4 January 2010 / Accepted: 8 May 2010 / Published online: 20 May 2010

Abstract Zirconia–5 mol% yttria has been used successfully for pH sensing in high temperature water (≥300 °C). However, this material, which consists of the cubic phase with 2–8 vol.% intergranular tetragonal precipitates, is not always stable in this environment and some batches were found to be fragmented by cracking within a few days. To study this effect, different samples of the material were structurally characterised and exposed to 300 °C water. It was found that the susceptibility to cracking increased with the volume content of the intergranular precipitates. The cracking mechanism was explained by the stress-induced grain boundary cracking of the cubic phase, the stress being due to the water-induced martensitic transformation of the tetragonal precipitates. A model has been proposed which allows to interpret the dependence of crack formation propensity on the size of the tetragonal precipitates.

Introduction

As a consequence of its good oxygen ion conductivity stabilised or partially stabilised zirconia (PSZ) is used as solid electrolyte in oxygen sensors operating in a high temperature environment. As described previously, tubes of zirconia with 5 mol% yttria are being used in an experimental pH sensor developed for high temperature water: 300 °C–150 bar [1]. The main reason for the selection of this composition was its commercial availability. Experience with this material showed that in general the tubes survive this environment for more than 500 h. However, some batches were found to be completely fragmented after 24 to a few 100 h exposure. The present study was performed to find an explanation for this phenomenon.

To understand the structure of the present material, the zirconia-rich part of the phase diagram should be considered [2–4]. In the temperature range where sintering is generally done (1200–1700 °C) the three domains of interest are, from low to high yttria content: the tetragonal (T) phase domain, the coexistence domain of the tetragonal and cubic (C) phases and the cubic phase domain. On cooling below the M_s temperature or under the influence of a stress the tetragonal phase may transform by a martensitic mechanism to the monoclinic (M) phase.

A huge amount of research has been carried out on ceramics consisting of around 3 mol% yttria. They are known as tetragonal zirconia polycrystalline (TZP) materials since their martensitic transformation is inhibited by the small grain size [5]. However, Kobayashi was the first to report their degradation by cracking upon ageing in air for 3000 h at temperatures of 100–300 °C [6]. Later work showed that ageing in water shortened the degradation time to less than 100 h [7–10]. These early studies showed that cracking was caused by the volume expansion accompanying the martensitic transformation. It was supposed that water facilitates the formation of monoclinic nuclei. Unlike martensitic transformations in, e.g. steel, it was found that the transformation progresses isothermally, even at the surface which was in direct contact with water. This was ascribed to a time dependence of the nucleation process [5, 7–11]. Several possible time dependent interactions of water with the Y_2O_3–ZrO_2 ceramic have been proposed [8, 12–14].

W. Vandermeulen (✉) · R.-W. Bosch · A. Leenaers · W. Van Renterghem
Belgian Nuclear Research Center, Boeretang 200, 2400 Mol, Belgium
e-mail: wvanderm@sckcen.be

F. Snijkers
Flemish Institute for Technological Research, Boeretang 200, 2400 Mol, Belgium

A critical review, together with a model based on the grain boundary diffusion of OH^- ions and the interaction of the latter with oxygen vacancies can be found in [15].

Much less research was performed on compositions with more than 3 mol% yttria. Some studies showed that for these materials, when sintered in the range 1500–1700 °C, the sensitivity to cracking in water decreased with increasing yttria content [5–7]. The scarce micrographs of these materials show a continuous tetragonal phase network that obviously provides a path for crack propagation by martensitic transformation. Since the yttria content of the tetragonal phase should be the same for all materials sintered at the same temperature in the T + C domain, the decreased degradation sensitivity can only be explained by a decrease of the amount and size of the tetragonal phase and/or by the tetragonal network becoming discontinuous.

The cubic phase has generally been considered as being stable in high temperature water [16]. Only more recently it was reported to show cracking after 2 years exposure to water vapour at 250 °C [17]. In this case cracking was found to be slow and transgranular. In the materials considered in the present study the tetragonal precipitates are either completely isolated from each other or occur in isolated clusters. Thus, no continuous network is present for crack propagation. This is probably the reason why in general no degradation occurs within times of hundreds of hours. Nevertheless, fast grain boundary cracking occurred in some batches. This appears to be a phenomenon that has not been described yet. In the following sections, it will be further discussed and related to the amount of intergranular tetragonal precipitates.

Experimental procedure

All samples were cut with a diamond disk from commercially available 3 × 6 or 5 × 7.5 mm diameter tubes of nominally 5 mol% yttria–zirconia. No manufacturer information on the sintering conditions and the amount of additives and impurities is available. After a preliminary autoclave test three material types were selected: material A represents the most common type, showing no failure within 750 h; material B has a high propensity to cracking; material C has a very high propensity for cracking. These materials were thoroughly characterised and subjected to new autoclave tests.

The autoclave tests were performed in an environment simulating the conditions in a nuclear pressurised water reactor, i.e. demineralised water containing 1000 ppm B as $B(OH)_3$ and 2 ppm Li as LiOH. All tests were done at 300 °C for times of 24 to 750 h. Heating or cooling took about 5 h.

Polished sections were obtained by grinding on SiC paper up to 1200 grit size and polishing to 1 μm grit diamond. Etching was done at room temperature in a 45/10/45 vol.% $HNO_3/H_2O/HF$ mixture for 10 to 30 min [18]. The structure was observed by means of an optical microscope (OM) and a scanning electron microscope (SEM) equipped with an energy dispersive analysis system (EDS). Transmission electron microscopy (TEM) with EDS was used to a limited extent.

After etching the size distribution of the tetragonal precipitates was determined. This had to be done in the OM since the SEM presented hardly any contrast between the tetragonal and cubic phases. Therefore, the analysis had to be limited to the optically visible particles (>1 μm). Since from the degradation model developed below follows that the contribution of submicron particles to the transformation stresses is small, the omission in these particles in the analysis is acceptable. As an approximation, it was assumed that the measured size distribution, biased by non-central cutting of the precipitates, is the same as the real size distribution [19]. Furthermore, for each precipitate an equivalent sphere with radius R was defined, having the same volume as the roughly ellipsoidal particle. Since it was observed that the larger precipitates or clusters of precipitates were nearly equiaxed, this simplification has no great effect on the semi quantitative explanation of the degradation. The number of precipitates per unit volume was calculated according to Modin [19].

The grain size distribution was determined by measuring the diameter of about 100 grains taken at random. No correction was applied to account for non-central sectioning [19]. The pore and alumina volume fractions were determined on SEM pictures according to standard CEN ENV 623-5:2002.

The fracture toughness was estimated by the Vickers indentation technique at 5 and 10 kgf loads using the expression which was first given by Anstis et al. [20]:

$$K_{\mathrm{Ic}} = 0.016(E/\mathrm{HV})^{1/2} F c^{-3/2} \quad (1)$$

where E is Young's modulus (200 GPa), HV Vickers hardness, F the indentation force and 2c the crack length, measured from tip to tip.

X-ray diffraction (XRD) patterns were obtained with a Cu X-ray tube on specimens of 4 × 10 × 0.5 mm^3 cut from the tube wall. These samples were polished as for optical examination. The small sample size, together with the grain size of 20–50 μm prevented quantitative analysis of the diffraction patterns.

Results

Structure of the as-sintered materials

The zirconia phases present in the different materials were identified by means of XRD. As an example, the lower

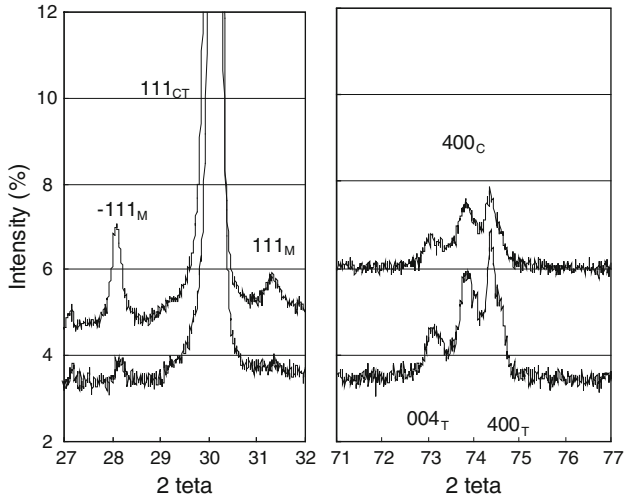

Fig. 1 XRD (Cu Kα) patterns of material B, as received (*lower curves*) and after autoclave exposure for 24 h (*upper curves*). Cubic (*C*), tetragonal (*T*) and monoclinic (*M*) phase peaks have been indicated. *T* indices refer to pseudo cubic unit cell

curves in Fig. 1 show the two most relevant regions of the XRD pattern of material B in the as-sintered condition. The region around 30° 2θ shows one single peak formed by the overlapping (111) tetragonal and cubic phase reflections. Very weak monoclinic phase peaks can be seen. This was similar for material C. Material A did not show monoclinic peaks. It was not clear whether the monoclinic phase is present after sintering or induced by the specimen cutting and polishing. The volume ratio of the cubic and tetragonal phases is generally estimated from the peaks near 73° 2θ. Because of the limited sample size no attempt was made to determine this ratio quantitatively. However, comparison with similar XRD patterns found in literature [21] shows that both phases are present in roughly equal amounts in the three material types.

The results of the OM and SEM observations, as discussed below, are summarised in Table 1. This table shows the grain size, pore volume and volume of alumina and intergranular tetragonal particles. It further gives details related to the size distribution of the latter and finally the fracture toughness values. For each material type two or three areas were examined. The data for each area are given separately in the table in order to provide some indication about the inhomogeneity of the structure. The microscopic observations will be discussed below.

SEM examination of unetched polished cross-sections shows three types of structural features (Fig. 2): pores with diameters up to about 5 μm; second-phase particles, showing dark contrast relative to the matrix and some dark, serpentine shaped zones, about 0.5 μm thick, extending along grain boundaries. EDS showed the second-phase particles to be nearly pure alumina. Analysis of the serpentine-like zones was not possible because of their limited thickness.

After etching, two additional structural features can be seen as shown by the OM pictures in Fig. 3: the grain boundaries and a population of precipitates, which are almost exclusively lying at the grain boundaries. EDS analysis showed these precipitates to have a lower yttrium content compared with the surrounding grains. It thus can be concluded that they consist of the tetragonal phase while the surrounding grains consist of the cubic phase. However,

Table 1 Structural characteristics of the materials A, B and C: grain size, vol.% of pores and alumina particles

Material type/area[a]	Grain diameter (μm)	Pores (vol.%)	Alumina (vol.%)	Tetragonal phase (vol.%)	Number of T particles (mm^{-3})	Equivalent particle diam (μm)	T particles per grain	Fracture toughness (MPa $m^{0.5}$)
A/1	43	1.4	2.5	1.5	902,000	3.1		
A/2	45	1.6	2.8	2.3	849,000	3.7		
Mean A	44	1.5	2.7	1.8	875,000	3.4	40	2.8[b]
B/1	36	4.1	2.7	2.9	72,000	9.2		
B/2	37	4.4	2.9	1.9	284,000	5.0		
B/3		4.7	3.1	3.9	162,000	7.7		
Mean B	37	4.4	2.9	2.8	173,000	7.3	5	3.6[b]
C/1	21	5.3	4.3	5.5	113,000	9.8		
C/2	18	4.2	4.1	7.7	105,000	11.2		
C/3	21	4.9	4.2	9.9	110,000	12.0		
Mean C	20	4.9	4.2	7.8	109,000	11.0	0.5	4.3[b]

Parameters characterizing the population of intergranular tetragonal precipitates (T): vol.%, number of precipitates per mm^3 and equivalent T particle diameter and number of particles per cubic phase grain. Average fracture toughness determined by hardness indentation

[a] Numerals indicate micrograph number

[b] Standard deviation about 0.5 MPa $m^{0.5}$

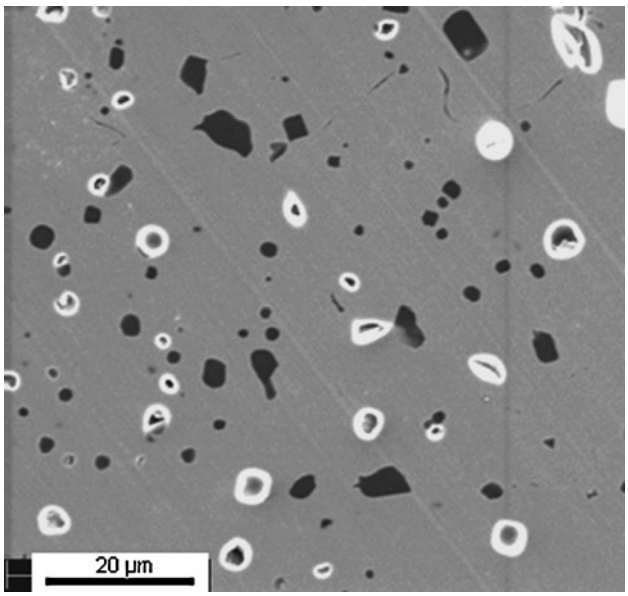

Fig. 2 Unetched section (SEM) of material B showing pores (*white halo*), alumina particles (*dark*) and serpentine like phase along some grain boundaries (*dark*, *upper region*)

these precipitates do not account for the roughly 50 vol.% of tetragonal phase estimated from the XRD patterns. This deficiency will be explained below. From Fig. 3 it can be seen that the tetragonal particles in materials B and C are considerably larger than those in material A. This is quantified by Fig. 4, which shows the cumulative tetragonal precipitate number density versus size. The average size, calculated from the measured volume fraction and number density, increases and the particle number density decreases from A to C (Table 1). The average volume fraction of the intergranular tetragonal precipitates is, respectively, around 2, 3 and 8% but it varies with a factor of about two from one location to another. From the precipitate density and the matrix grain size the number of precipitates per grain was calculated to be about 40, 5 and 0.5 for materials A, B and C, respectively. As will be shown later these ratio's help to explain differences in cracking behaviour. From Table 1 it can be seen that grain size, porosity and volume fraction of alumina particles are homogeneous within each material although they vary between the three material types.

At magnifications above 2000 times SEM of strongly etched samples showed that the cubic grains contain a high density of submicron precipitates. To determine the nature of these precipitates, a material A sample was examined by TEM. Bright field imaging showed precipitates of around 50 nm (Fig. 5). The insert of the figure shows a diffraction pattern including matrix and precipitates. Overlapping cubic and tetragonal phase spots can be seen with in between them weaker spots characteristic of the tetragonal phase [22]. Dark field imaging showed the precipitates to

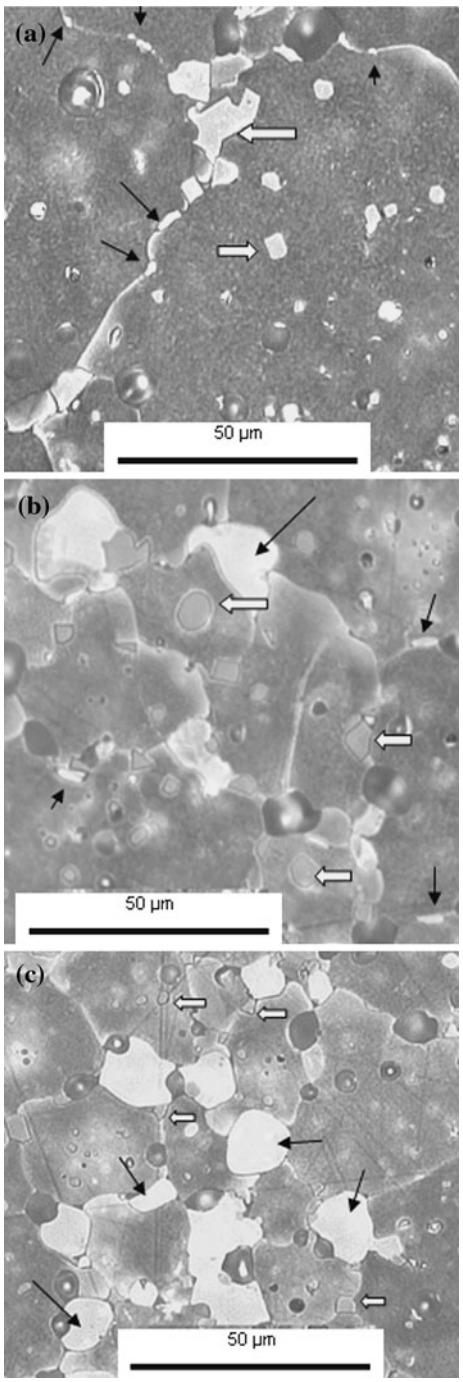

Fig. 3 Etched sections (OM) of materials A (**a**), B (**b**) and C (**c**). *White arrows* indicate alumina particles, *black arrows* indicate intergranular tetragonal precipitates

consist of the tetragonal phase. It can be seen that the cubic and tetragonal phases are present in roughly equal amounts. This corresponds well with the XRD observations and explains the tetragonal phase deficiency found by OM.

At some triple grain junctions a glassy phase, rich in silicon, was seen by TEM. This might be the same as the serpentine-like phase observed by SEM. However, the

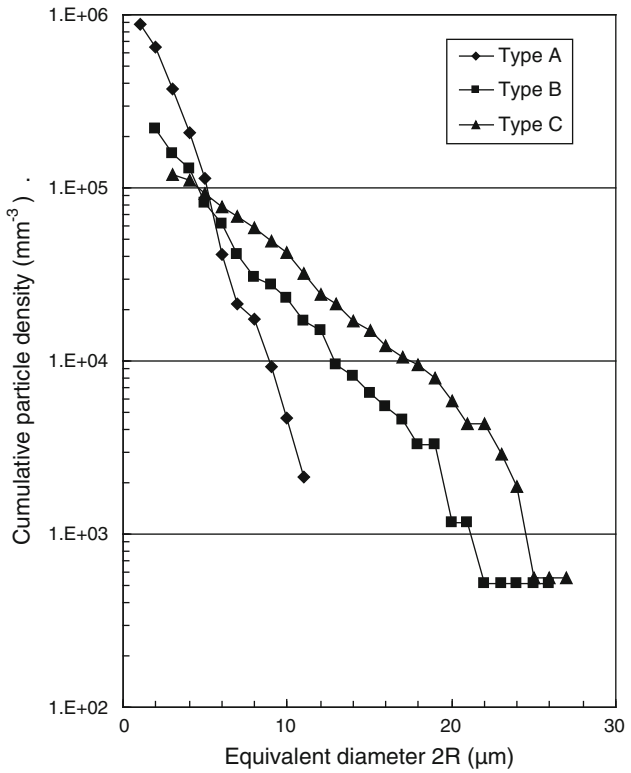

Fig. 4 Cumulative size distribution of the intergranular tetragonal precipitates in the three material types

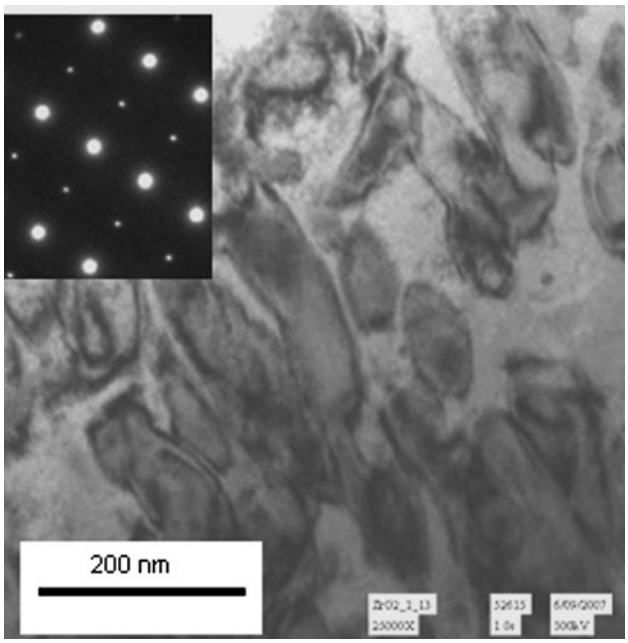

Fig. 5 Bright field TEM picture of as-received material A showing submicron intragranular tetragonal precipitates. The intense spots in the diffraction pattern are due to the tetragonal and cubic phases and the weak ones are due to the tetragonal precipitates

latter shape was not found by TEM, probably because of the limited area which could be examined. The grain boundaries were inspected for the existence of an amorphous layer but this was not found. The reason for this could be the difficult observational conditions. It therefore cannot be excluded with certainty that a nanometer scale amorphous layer, as observed in TZP by some workers, is present [23, 24]. On the other hand, it may be that no layer is present since grain boundaries *without* amorphous layer have been reported to exist in TZP as well as in 8 mol% yttria cubic zirconia [25].

Fracture toughness

The fracture toughness measurements show a rather wide scatter because of the coarse grain size, the occurrence of chipping and crack arrest by particles and pores. The average values for the three materials, 3 to 4 MPa $m^{0.5}$ (Table 1), are higher than the value of 1.5 MPa $m^{0.5}$ reported for 8 mol% yttria tested by indentation [26]. This difference may be due to the toughening effect of the fine precipitates in the cubic matrix. It should be emphasised that all indentation cracks are transgranular. This means that in air at room temperature the grain boundaries have a higher fracture toughness than the grain interior.

Degradation observations after autoclave exposure at 300 °C

Polished samples of materials A, B and C were first exposed for 24 h together with the specimens for XRD. After exposure, OM and SEM showed that the intergranular tetragonal precipitates have become visible without etching because their surface had become irregular as compared to the surrounding cubic grains. Furthermore, some of them were more reflective in the OM because of subsurface cracking. These observations are an indication for the martensitic transformation of these particles. Materials A and B showed cracking along a limited number of grain boundaries. Material C showed extensive intergranular cracking. A section of the latter revealed that it was completely fragmented, almost down to the size of the cubic grains.

The upper curves in Fig. 1 show the XRD pattern of material B after the 24 h exposure. Although the monoclinic peaks in the patterns of the three materials have increased, they are still weak. The relative intensity of the cubic and tetragonal peaks has not changed significantly. Therefore, it can be concluded that the martensitic transformation was limited to the larger, i.e. intergranular precipitates while the submicron *intragranular* precipitates, which are estimated to constitute the largest fraction of the tetragonal phase, remained untransformed.

Because it was found that cutting and grinding of exposed material C caused additional cracks, the study of the cracking evolution in the three materials was started again. This time the transition from transgranular to intergranular cracking was followed on fracture surfaces obtained by breaking tube segments after exposure. This was done at room temperature on specimens shaped to a C-ring. The results are discussed below.

In the as-received condition the fracture mode of the three materials was found to be completely transgranular. This fracture mode was also found at the hardness indentations.

After 24 h up to 750 h exposure the appearance of the fracture surface of material A is the same. Fracture is largely transgranular but small regions with intergranular fracture occur at the section corners (Fig. 6). It was estimated that the transgranular fracture occurred by post exposure breaking and that the intergranular cracks had formed during exposure.

After 24 h exposure, the fracture surface of material B was similar to material A except that the intergranular regions were larger. With increasing exposure time these regions were found to grow. After 440 h and up to 750 h fracture was completely intergranular with only some small transgranular facets across single grains (Fig. 7). In this stage, breaking a specimen merely separates the two parts along intergranular cracks formed during exposure. No new fracture surfaces are formed, except for the few grains which break transgranularly, due to local stress concentrations.

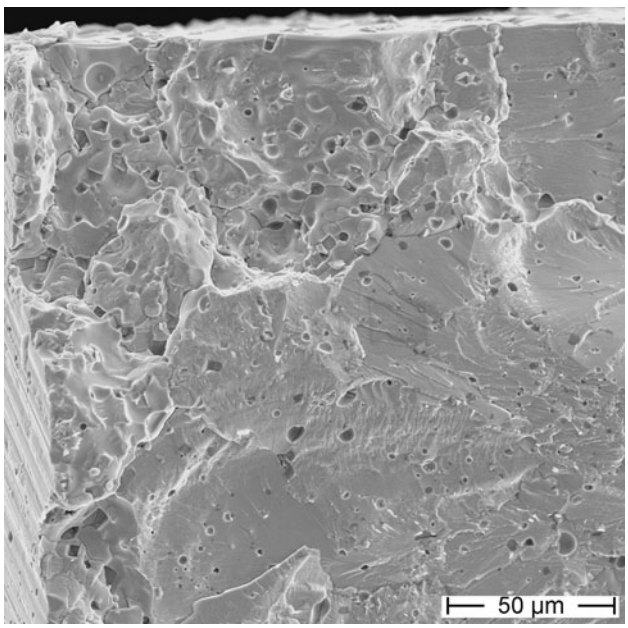

Fig. 6 Material A, broken after 750 h autoclave exposure. Intergranular fracture (*upper left region*) and transgranular fracture (*right*)

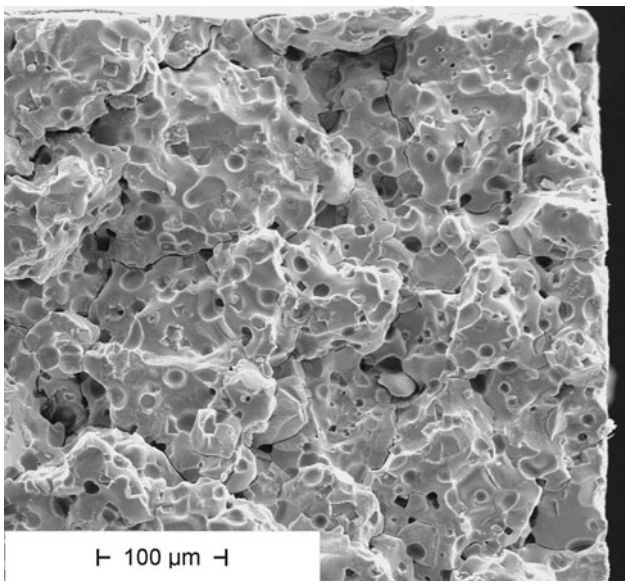

Fig. 7 Material B, broken after 750 h autoclave exposure. Intergranular fracture over complete surface

The fracture surfaces of material C, broken after 24 or 115 h exposure, were largely transgranular but similar to material B, intergranular fracture zones occurred at the saw cut edges. In the latter regions the grain size, determined by measuring the grains on the fracture surface is nearly the same as the size obtained from an etched section. This shows that cracks have formed along *all* grain boundaries. In the transgranular region it was found that, as opposed to materials A and B, a network of intergranular cracks intersected the fracture surface (Fig. 8). The size of the blocks formed by this crack network is on the average twice the grain size. This means that in this region cracks have not yet formed along all grain boundaries. Since the cracks emerging at the fracture surface are perpendicular to it and intergranular, it is unlikely that they were created by breaking the sample. Therefore, they must have been formed during exposure. The transgranular fracture surface on the contrary is thought to have formed by breaking the sample since if breaking had occurred along the pre-existing crack network the surface should have been much more irregular. Clearly in this region the different blocks were too strongly interlocked to allow the simple separation observed in the intergranular fracture region.

From the foregoing it was concluded that in material C crack formation occurs in two stages. In the first stage the coarse intergranular crack network is expected to form throughout the sample within 24 h. The mesh size of this network is about twice the grain size. In the second stage cracking occurs along the yet uncracked grain boundaries. This stage takes more than 100 h. Unfortunately it could not be followed beyond 115 h but it is likely that at longer

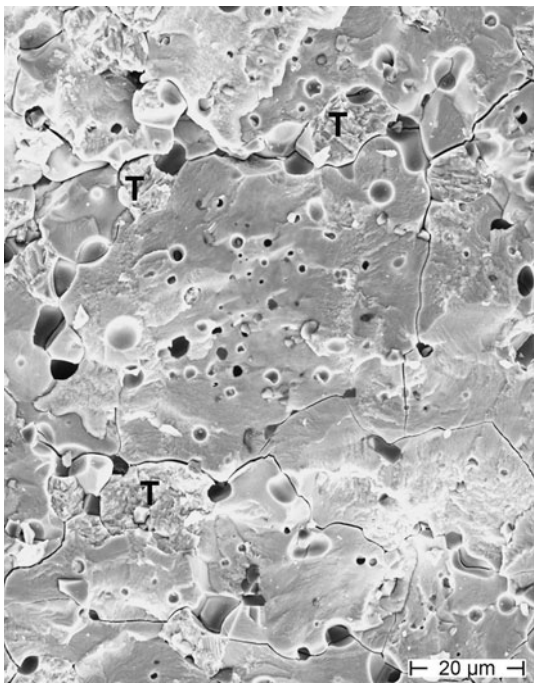

Fig. 8 Material C, broken after 24 h autoclave exposure. Transgranular fracture surface intersected by intergranular crack network and transformed tetragonal precipitates (*T*)

times intergranular cracking would extend along all grain boundaries, similarly to material B.

Discussion

Structure

The three materials consist mainly of grains with a cubic crystal structure. Within these grains a high density of submicron tetragonal precipitates, occupying roughly half of the grain volume, is found. Intergranular tetragonal precipitates occupy 2 to 8% of the total volume, depending on the material type. These precipitates have sizes up to 25 µm. Pores and alumina particles occur, both with volume fractions of 2–5%. A glassy phase of about 0.5 µm thickness extends along some grain boundaries. The large intergranular precipitates are thought to have formed together with the cubic phase at the sintering temperature. The fine intragranular precipitates probably have formed during cooling. Similar precipitates have been described for magnesia [27, 28] and yttria [29] stabilised zirconia. Because information on the sintering conditions was not available, finding an explanation for the structural differences between the three material types was considered outside the scope of this study. Since the pores and the alumina particles do not seem to play a role in the degradation process, attention will be focused on the intergranular tetragonal precipitates.

Degradation

From the exposure tests follows that in the present materials contact with 300 °C water (1) causes the martensitic transformation of the larger, mainly intergranular, tetragonal precipitates, a phenomenon well-documented [6–11] and (2) leads to intergranular cracking of the mainly cubic-cubic grain boundaries. Apparently water induces a mechanism that allows these cracks to grow at a stress intensity lower than the critical stress intensity for transgranular fracture. Comparison of the three material types shows that the propensity for grain boundary cracking increases with the size and/or volume fraction of the intergranular precipitates. It therefore can be concluded that the stress field around the transformed precipitates, caused by the 3% volume expansion [30, 31], acts as the driving force for the cracking mechanism. Unfortunately, from the present tests it was not possible to deduce a mechanism by which water attenuates the grain boundary strength. Therefore, in the further discussion the phenomenon of grain boundary cracking will be taken for granted and attention will be paid to the general failure mechanism and the quantification of its dependence on the size of the tetragonal precipitates.

To explain the general failure mechanism a highly simplified two-dimensional model was used. It was assumed that all intergranular precipitates have the same diameter $2R$ and are located at the corners of a square lattice with constant d (Fig. 9). As shown in this figure, fracture is supposed to be initiated by the transformation of the intergranular precipitates at the surface of a plate specimen exposed on both sides. The cracks generated are

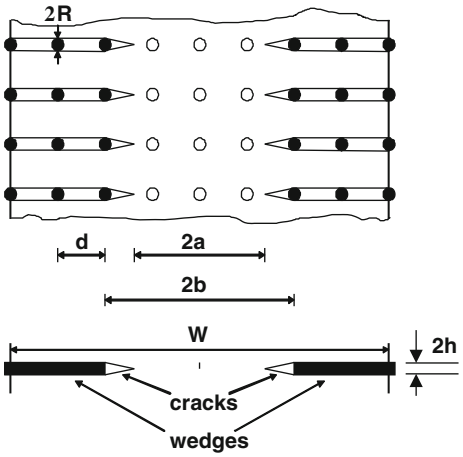

Fig. 9 *Upper part* schematic representation of cracks propagation in a plate specimen with thickness *W* exposed on both sides. *Black circles* represent transformed precipitates; *open circles* represent untransformed precipitates. *Lower part* single crack set with wedges replacing the effect of transformed precipitates. The relevant geometrical parameters for the calculation of K_I are indicated

expected to grow along a grain boundary to the nearest subsurface precipitate. Once this is reached by the crack it is supposed to transform because of the contact with water and/or by the crack tip stress field. Its expansion provides a new driving force for crack growth. This process can in principle continue until all grain boundaries have cracked.

Since the driving force for crack growth is conveniently represented by the stress intensity factor K_I it was attempted to calculate the latter for a crack starting from a transformed precipitate. A model for this case was already presented by Green [32]. In this model the stress field around a particle in the absence of a crack is used to calculate the stress intensity for a radial crack. Hereby it was acknowledged that relaxation of the stress field due to the crack formation was not taken into account. This leads to a stress intensity factor which is zero for very short cracks and which increases with increasing crack size. However, in the *actual* situation it is not the stress field that is imposed but the displacement at the crack origin, caused by the expansion of the transforming particle. This situation can be described as a crack opened by a wedge, the wedge thickness being equal to the linear expansion. To be precise the wedge thickness should be corrected for elastic compression by the crack flanks. In the present calculations this correction has not been applied. This means that the stress intensity is overestimated for short cracks. For long cracks the correction becomes negligible because of the increasing crack compliance.

In the Appendix, an expression given by Tada for cracks opened by wedges is used to express K_I as a function of crack length and average precipitate size. The lower curves in Fig. 10 show the result for the three material types. As opposed to the result obtained by Green it is found that K_I decreases with increasing crack length. The transgranular K_{Ic} values from Table 1 are indicated as well. It is clear that according to the present model, transgranular crack lengths should remain below around 2 μm. Even at the largest precipitates ($2R = 25$ μm in material C), transgranular cracks should remain shorter than about 5 μm (Fig. 10, bold curve). These results agree well with the fact that no transgranular cracking occurs during exposure. They also justify the use of the room temperature/air K_{Ic} values in Fig. 10. If the transgranular 300 °C/water K_{Ic} values would have been much lower than the room temperature/air ones at least *some* degree of transgranular cracking would have occurred *during* exposure.

Figure 10 further shows that to explain the formation of intergranular cracks of the order of the grain size (20–50 μm) within periods of some 100 h the cracking mechanism should be operational at stress intensities around 1 MPa $m^{0.5}$. In order to explain the different cracking propensity of the three materials it was assumed that the crack growth rate V along the grain boundaries is of the form:

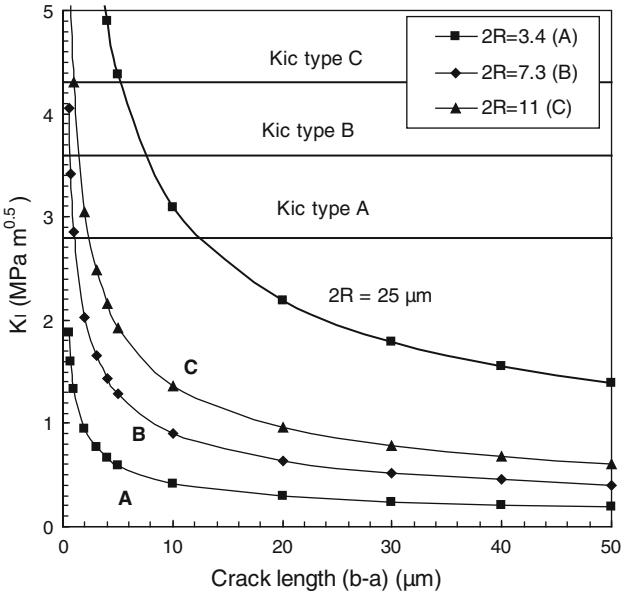

Fig. 10 K_I vs. crack length in materials A, B and C (*three lower curves*) and for precipitates of 25 μm diameter (*upper curve*). The *horizontal lines* indicate the room temperature/air transgranular fracture toughness of the three materials. The expected transgranular crack length in each material is given by the intersection of the K_I curve and the corresponding *horizontal line* representing K_{Ic}

$$V = cK_I^m \tag{2}$$

This is the general expression for crack growth in glasses [33, 34] but it is likely to apply to any stress-assisted mechanism. Supposing m is much larger than one, as in the case of glasses, V increases quickly for K_I above 1 MPa $m^{0.5}$ and decreases rapidly below that value.

Figure 10 shows that the average precipitate size in material C causes a K_I value above 1 MPa $m^{0.5}$ for cracks up to 20 μm, i.e. the grain size. Rapid crack growth thus can be expected up to 20 μm. However, since on the average only one tetragonal precipitate is available for two grains (Table 1) initial rapid crack growth can only be expected along a fraction of the grain boundaries. This explains the formation of the crack network with coarse mesh size within 24 h. Formation of this network is expected to relax the stress field and to decrease K_I below 1 MPa $m^{0.5}$ so that further crack growth is slow. In this stage the cracks may further extend along the precipitate free grain boundaries. Figure 10 shows that in material B fast crack growth would be limited to crack lengths of about 10 μm. This is clearly not sufficient to form a crack network within some 24 h. This is why cracks spread along all grain boundaries simultaneously, but at a rate that requires several 100 h. Finally, in material A, with the exception of a few small regions, the stress field is clearly unable to cause even slow crack growth.

Conclusions

The degradation of the present 5 mol% yttria stabilised zirconia can be explained by the combination of two water-induced effects. The first is the martensitic transformation of the intergranular tetragonal precipitates. The second is the appearance of a stress assisted intergranular cracking mechanism. The increasing susceptibility to degradation of the three material types could be explained by a model based on wedge opened cracks, with the wedge thickness depending on the average precipitate size.

Appendix

In this section, the stress intensity factor K_I is calculated for a crack ahead of a row of transformed precipitates as shown in Fig. 9. The distance between the transformation fronts approaching each other from both sides of the sample is $2b$ and the distance between the crack fronts is $2a$. Therefore, the crack ahead of the last transformed particle has a length $(b - a)$. This crack has to grow to a length d to reach the next particle. It follows that $(b - a)$ values up to the interparticle distance, i.e. about 50 μm, have to be considered.

The lower part of Fig. 9 schematises the geometry by replacing the effect of the transformed particles by wedges of thickness 2 h inserted from both surfaces up to the innermost transformed particle. For this configuration, consisting of two wedges in a *finite* thickness plate no analytical expression for K_I was found. However, a solution for two wedges in an *infinite* specimen has been given by Tada [35]. This has been used since it is thought to be a good approximation, provided the wedge insertion depth is sufficient for surface proximity to be negligible.

The stress intensity factor given by Tada for the configuration shown in the lower part of Fig. 9, is as follows:

$$K_I = \frac{Eh\left(\frac{\pi}{a}\right)^{0.5}}{2kK(k)} \tag{3}$$

where E is Young's modulus (200 GPa), h is the half wedge thickness, a is defined above and K is a function of k tabulated in Appendix J.1 of [35] and

$$k = \left[1 - \left(\frac{a}{b}\right)^2\right]^{0.5}. \tag{4}$$

Cracks growing from a transformed to an untransformed particle have a length $(b - a)$ which is always shorter than the interparticle spacing d. This means that, except for very small ligament sizes, a/b is close to 1 and k is close to zero. This allows to approximate (4) as

$$k = \left[2\left(1 - \frac{a}{b}\right)\right]^{0.5}. \tag{5}$$

For small k, $K(k)$ is nearly constant and equal to 1.6. After modification, (3) can then be written as

$$K_I = 0.392\frac{Eh}{(b-a)^{0.5}}. \tag{6}$$

There is no obvious way to express h as a function of precipitate size and distribution. To avoid this problem h was calculated supposing the average equivalent particle diameter $2R$ (Table 1) to determine the wedge height 2 h. Supposing that the particles show an isotropic linear expansion of 1.0% [29, 30], the expression for h is

$$h = 0.01R. \tag{7}$$

Introducing (7) in equation (6) gives K_I as a function of crack size $(b - a)$ and average precipitate diameter $2R$

$$K_I = 0.00196\frac{E(2R)}{(b-a)^{0.5}}. \tag{8}$$

Equation (8) was used to calculate the curves in Fig. 10.

It is acknowledged that considerable simplifications were necessary to arrive at expression (8). For example, only cracks perpendicular to the sample surface are considered, whereas in reality cracks occur in all directions. Furthermore, the precipitate density does not appear in the final expression. The absolute values for the stress intensity factor therefore should be considered with caution. However, the simplifying assumptions should affect the *ranking* of the three material types to a much lesser degree. The conclusion that the cracking propensity is dependent on the size of the intergranular tetragonal precipitates is therefore likely to be acceptable.

References

1. Bosch R-W, Wéber M, Vandermeulen W (2009) Power Plant Chem 11:30
2. Scott HG (1975) J Mater Sci 10:1527. doi:10.1007/BF01031853
3. Stubican VS, Hink RC, Pray SP (1978) J Am Ceram Soc 61:17
4. Heuer H, Rüle M (1984) In: Claussen N, Rühle M, Heuer HA (eds) Advances in ceramics, vol 12, Proceedings of international conference on the science and technology of zirconia II, Stuttgart 1983. American Ceramic Society, Columbus, OH
5. Sato T, Ohtaki TS, Shimada M (1985) J Mater Sci 20:1466. doi:10.1007/BF01026344
6. Kobayashi K, Kuwajima H, Masaki T (1981) Solid State Ionics 3–4:489
7. Nakajima K, Kobayashi K, Murata Y (1984) In: Claussen N, Rühle M, Heuer HA (eds) Advances in ceramics, vol 12, Proceedings of international conference on the science and technology of zirconia II, Stuttgart 1983. American Ceramic Society, Columbus, OH
8. Sato T, Shimada M (1985) J Am Ceram Soc 68:356

9. Chevalier J, Cales B, Drouin JM (1999) J Am Ceram Soc 82:2150
10. Pyyapilly PP, Butt DP (2007) J Nucl Mater 360:92
11. Kim D, Jung H-J, Cho D-H (1995) Solid State Ionics 80:67
12. Lange FF (1986) J Am Ceram Soc 69:240
13. Guo X (1999) J Phys Chem Solids 60:539
14. Yoshimura M, Noma T, Kawabata K, Somiya S (1987) J Mater Sci Lett 6:465
15. Guo X (2004) Chem Mater 16:3988
16. Guo X (2000) Phys Status Solidi (a) 177:191
17. Guo X, He J (2003) Acta Mater 51:5123
18. Annamalai VE, Gokularathnam CV, Krishnamurthy R (1992) J Mater Sci Lett 11:824
19. Modin H, Modin S (1973) Chap. 5 in Metallurgical Microscopy. Butterworth, London
20. Anstis R, Chantikul P, Lawn BR, Marshall DB (1981) J Am Ceram Soc 64:533
21. Miller RA, Smialek JL, Garlick RG (1981) In: Heuer AH, Hobbs LW (eds) Advances in ceramics, vol 3, Proceedings of 1st international conference on the science and technology of zirconia, Cleveland, OH, 1980. American Ceramic Society, Columbus, OH
22. Lanteri V, Heuer HA, Mitchell TE (1984) In: Claussen N, Rühle M, Heuer HA (eds) Advances in ceramics, vol 12, Proceedings of international conference on the science and technology of zirconia II, Stuttgart 1983. American Ceramic Society, Columbus, OH
23. Tsubakino H, Fujiwara T, Satani K, Ioku S (1997) J Mater Sci Lett 16:1472
24. Gremillard L, Epicier T, Chevalier J, Fantozzi G (2005) J Eur Ceram Soc 25:875
25. Matsui K, Yoshida H, Ikuhara Y (2008) Acta Mater 56:1315
26. Tekeli S (2006) Mater Des 27:230
27. Porter L, Heuer AH (1979) J Am Ceram Soc 62:298
28. Montross CS (1992) J Am Ceram Soc 75:463
29. Matsui M, Soma T, Oda I (1984) In: Claussen N, Rühle M, Heuer HA (eds) Advances in ceramics, vol 12, Proceedings of international conference on the science and technology of zirconia II, Stuttgart 1983. American Ceramic Society, Columbus, OH
30. Kriven WM, Fraser WL, Kennedy SW (1981) In: Heuer AH, Hobbs LW (eds) Advances in ceramics, vol 3, Proceedings of 1st international conference on the science and technology of zirconia, Cleveland, OH, 1980. American Ceramic Society, Columbus, OH
31. Rühle M, Heuer HA (1984) In: Claussen N, Rühle M, Heuer HA (eds) Advances in ceramics, vol 12, Proceedings of international conference on the science and technology of zirconia II, Stuttgart 1983. American Ceramic Society, Columbus, OH
32. Green DR (1981) J Am Ceram Soc 64:138
33. Dériano S, Jarry A, Rouxel T, Sangleboeuf J-C, Hampshire S (2004) J Non-Cryst Solids 344:44
34. Sakaguchi S, Sawaki Y, Abe Y, Kawasaki T (1982) J Mater Sci 17:2878. doi:10.1007/BF00644665
35. Tada H, Paris P, Irwin G (1973) The stress analysis of cracks handbook. DEL Research Corporation, St. Louis